IEEE Photonics Journal
An IEEE Photonics Society Publication

Open Access

Phase Alignment With Minimum Complexity for Equal Gain Combining in Multi-Aperture Free-Space Digital Coherent Optical Communication Receivers

Volume 12, Number 2, April 2020

Yicong Tu
Sheng Cui
Keji Zhou
Deming Liu

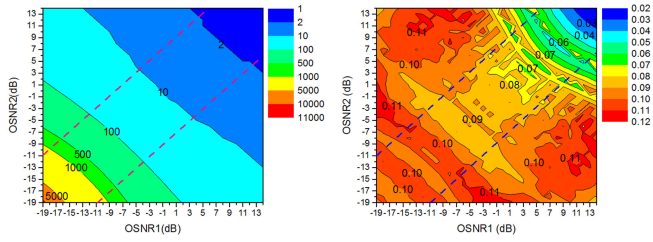

DOI: 10.1109/JPHOT.2020.2977955

IEEE photonics SOCIETY
IEEE

Phase Alignment With Minimum Complexity for Equal Gain Combining in Multi-Aperture Free-Space Digital Coherent Optical Communication Receivers

Yicong Tu,[1,2] Sheng Cui ,[1,2] Keji Zhou,[1,2] and Deming Liu[1,2]

[1]Wuhan National Laboratory for Optoelectronics, and School of Optical and Electronic Information, Huazhong University of Science & Technology, Wuhan 430074, China
[2]National Engineering Laboratory for Next Generation Internet Access System, Wuhan 430074, China

DOI:10.1109/JPHOT.2020.2977955

Manuscript received January 25, 2020; revised February 20, 2020; accepted February 28, 2020. Date of publication March 3, 2020; date of current version March 26, 2020. This work was supported by the National Natural Science Foundation of China (NSFC) under Grants 61975059 and 61975063. Corresponding author: Sheng Cui (e-mail: cuisheng@hust.edu.cn).

Abstract: Digital coherent combining (DCC) technique can increase the free space optical signal collection area by combining the signals received by an array of small apertures in a coherent manner. To realize DCC the different versions of signals must be aligned in phase by the digital phase alignment algorithm (PAA). Low computation complexity is imperative for the PAA because the main obstacle to implement the PAA and DCC in a real-time manner is the availability of digital signal processing (DSP) circuits offering very high gate density and processing speed. In this paper we investigate the relationship between the computation complexity, optical phase offset estimation error and the combining loss for the equal gain combining technique. Analytical expressions are deduced allowing easy minimization of the computation complexity at an arbitrary input OSNR and acceptable combining loss. Extensive numerical simulations are carried out to validate the analytical expressions.

Index Terms: Multi-aperture free-space optical communication receivers, phase alignment, digital coherent combining, minimum complexity, phase estimation error, combining loss.

1. Introduction

Free space optical communication can exploit the unregulated and nearly unlimited bandwidth in the near-infrared band and provide higher data rate and lower size, weight and power (SWaP) profile lasercom terminals compared to microwave communication. [1]–[5] For the satellite to ground downlink optical communication systems it is desirous to reduce the power-aperture product of the space-borne terminals by developing ground terminals with a large collection area. [6], [7] But large diameter telescopes are difficult to build and have focal plane thermal heating problem when operating in the day or pointing near the sun. [7], [10] Furthermore the light collected by the large diameter telescopes is difficult to efficiently deliver to a small area detector or single-mode fiber due to the atmospheric turbulence induced wave front distortion unless complex adaptive optics is employed. [11], [12] These problems can be solved by the coherent combining techniques

proposed recently [7]–[9]. They can increase the collection area by combining signals received by an array of small apertures in a coherent manner. When the aperture diameter is smaller than 5cm, adaptive optics correction beyond tip and tilt is rarely needed for a diffraction-limited single-mode receiver [7]. Furthermore the receivers employing multiple apertures can use spatial diversity to mitigate the atmospheric turbulence effect if the apertures are spaced apart by a distance much large than the atmosphere phase correlation length [7]–[9].

The coherent combining techniques proposed by now can be classified into two kinds [7]. The first kind of methods relies on analog approaches [13]–[17]. They need to realize optical path length matching between different branches down to a small fraction of a wavelength utilizing complex optical phase-locked loops (OPLL) [13]–[16] or fiber variable phase delays in combination with feed-back optical phase locking techniques [17]. The high optical complexity makes the scalability to a large number of signals difficult. The second kind of the methods relies on the digital coherent receivers (DCR) [7]–[9]. The optical signals received by different apertures are first detected by the DCRs. Their fields are recovered in the digital domain, and then coherently combined by the digital signal processing (DSP) system. The digital coherent combining (DCC) technique is appealing because instead of using the complex optics to stabilize the phase, it uses more robust and easier to implement digital time and phase alignment techniques. Experimental tests have shown that the DCC system can operate under a much lower input signal power (PPB $= -15$ dB) and tolerate a much larger optical path mismatch (more than 24 cm) [9]. The main obstacle for the real time implementation of the DCC technique is algorithm complexity and availability of DSP circuits offering very high gate density and processing speed. Therefore, all experiments to date had to resort to offline processing the sampled and stored received signals on a computer. DCC can employ maximal ratio combining (MRC), equal gain combining (EGC) or selection combining (SC) technique. EGC outperforms SC technique and gives comparable performance to MRC with reduced implementation complexity [20]. We will thus restrict the analysis to the EGC based DCC in this paper due to space limitation.

The algorithms used to realize DCC includes the time and phase alignment algorithms which aim at removing the time offset and optical phase offset (OPO) between the different versions of optical signals to be combined [7]–[9]. Due to the space limitation, we assume an ideal time alignment and focus on the phase alignment algorithm (PAA). Because PAA must deal with multiple high speed optical signals, reducing the PAA computation complexity is imperative for the real-time implementation of PAA and DCC using silicon devices. The problem to minimize the PAA computation complexity while guaranteeing an acceptable performance hasn't been discussed so far. In this paper we investigate the noise impact on the OPO estimation error and the combining loss which is defined with the ratio between the practical and theoretical OSNR values obtained after DCC. Analytical expressions for the OPO estimation error and combining loss are deduced. The use of analytical expressions permits easy minimization of the computation complexity at an arbitrary input OSNR and prescribed combining loss. The numerical simulations corroborate the analytical performance analysis. The paper is organized as follows. The analytical expressions are deduced in Section 2. Validating tests using numerical simulations are presented in Section 3. Conclusions are drawn in Section 4.

2. Phase Estimation Error and Combining Loss

The setup of the multi-aperture DCC receiver is shown in Fig. 1. Different versions of the free space optical signal received by different apertures are first amplified to overcome large free-space propagation losses and then detected by the parallel digital coherent receivers sharing a common narrow linewidth local oscillator (LO). The optical fields of the received optical signals are recovered in the digital domain, and then are aligned with each other in time and phase before being combined coherently in the DSP system. The flow chart of the phase alignment and coherent combining process is shown in Fig. 2. It operates by starting with one signal and coherently combining each subsequent signal with a running coherent sum of all previous signals. This architecture provides a greater SNR than the parallel or binary tree architecture [7]. The OPO (φ_n) between the two signals

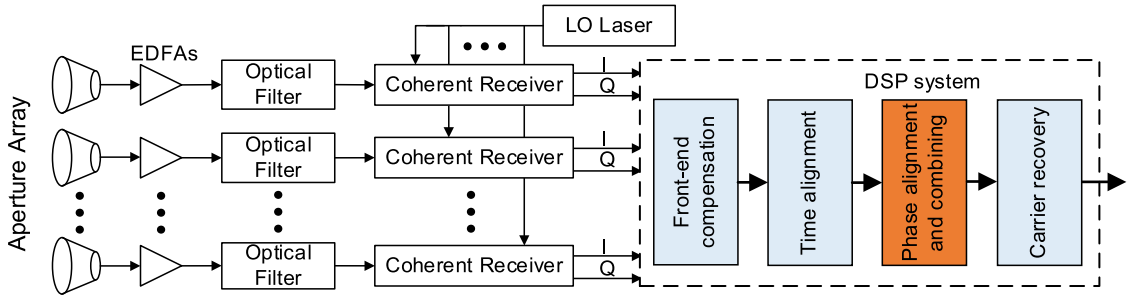

Fig. 1. The setup of the digital coherent combining receiver.

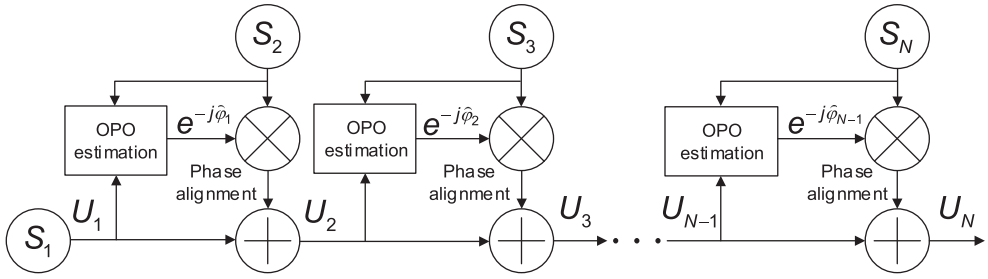

Fig. 2. The phase alignment and digital coherent combining process proposed in [7].

$(b_n,\ b_{n+1})$ to be combined is estimated using the following equations

$$C_{sum} = \sum_{m=1}^{M} b_{n+1}[m] \cdot \overline{b_n[m]}, \tag{1}$$

$$\hat{\varphi}_n = \arg\{C_{sum}\} = \varphi_n + \Delta\varphi_n. \qquad (1 \le n \le N-1) \tag{2}$$

Here $b_n[m]$ and $b_{n+1}[m]$ represent the m-th symbols of the two signals to be combined, respectively. M stands for the number of symbols used in the estimation. We note that the sampling rate is equal to the signal baud rate in the PAA. $\hat{\varphi}_n$ and $\Delta\varphi_n$ represent the n-th estimated OPO and the estimation error, respectively. N stands for the number of signals to be combined. As shown in Fig. 2 after $\hat{\varphi}_n$ is obtained, phase alignment is realized by multiplying the signal b_{n+1} with $e^{-j\hat{\varphi}_n}$.

Proper choice of M is vital for balancing the two competing requirements of low complexity and high estimation accuracy. To find the relation between $\Delta\varphi_n$ and M, we can begin with estimating the OPO between two optical signals (S_1, S_2) represented by

$$S_1 = A_1 e^{j(\phi_S + 2\pi\Delta ft + \phi_n)} + n_1,\ S_2 = A_2 e^{j(\phi_S + 2\pi\Delta ft + \phi_n)} \cdot e^{j\varphi_1} + n_2, \tag{3}$$

$$n_1 = I_1 + jQ_1,\ n_2 = I_2 + jQ_2. \tag{4}$$

Here φ_1 represents the OPO between $(S_1,\ S_2)$. $\phi_{s,n}$ are the modulated signal phase and laser phase noise, respectively. Narrow linewidth lasers are used to minimize the effects of laser phase noise so it is assumed to be the same for the corresponding symbols in $(S_1,\ S_2)$. Δf represents the laser frequency offset (LFO). n_1 and n_2 represent the ASE noise following complex Gaussian distribution. We note that they are independent random variables because they are generated by two different optical amplifiers. The real and imaginary parts (I_i and Q_i) of the ASE noise are thus independent identically distributed (i.i.d) random variables following Gauss distribution $N(0, \sigma_i^2)$.

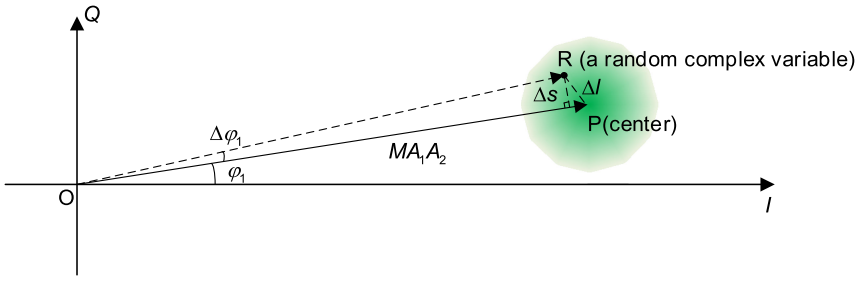

Fig. 3. The distribution of C_{sum} in a complex plane.

The variance σ_i^2 is related to the electrical and optical signal to noise ratio (SNR_i and $OSNR_i$) by the following equation [18]

$$\frac{A_i^2}{2\sigma_i^2} = SNR = OSNR \times \gamma. \tag{5}$$

Here γ is a calibration factor related to the signal bandwidth and modulation format. Substituting Eq. (3) into Eq. (1) we can obtain

$$C_{sum} = \sum^{M} S_2 \cdot \overline{S_1} = \sum^{M} \left(A_2 e^{j(\phi_S + 2\pi \Delta f t + \phi_n)} \cdot e^{j\varphi_1} + n_2\right)\left(A_1 e^{-j(\phi_S + 2\pi \Delta f t + \phi_n)} + \overline{n_1}\right)$$

$$= \sum^{M} \left(A_1 A_2 \cdot e^{j\varphi_1} + A_2\overline{n_1} + A_1 n_2 + \overline{n_1} n_2\right). \tag{6}$$

The last three items in the brackets represent the noise impact which incurs $\Delta\varphi_n$. We note that the pure phase factors in the noise items are neglected because they change neither the magnitude nor the statistical distribution of the noise. The real and imaginary parts of C_{sum} can be written as

$$I_{sum} = \sum^{M} \left(A_1 A_2 \cos\varphi_1 + A_2 I_1 + A_1 I_2 + I_1 I_2 + Q_1 Q_2\right), \tag{7}$$

$$Q_{sum} = \sum^{M} \left(A_1 A_2 \sin\varphi_1 - A_2 Q_1 + A_1 Q_2 - I_2 Q_1 + I_1 Q_2\right). \tag{8}$$

Their means and variances are as follows

$$E\left[I_{sum}\right] = MA_1 A_2 \cos\varphi_1, \quad E\left[Q_{sum}\right] = MA_1 A_2 \sin\varphi_1, \tag{9}$$

$$D\left[I_{sum}\right] = D\left[Q_{sum}\right] = M\left(A_1^2\sigma_2^2 + A_2^2\sigma_1^2 + 2\sigma_1^2\sigma_2^2\right). \tag{10}$$

Fig. 3 depicts the statistical distribution of the complex random variable C_{sum} on a complex plane. When noise is not present, $C_{sum} = MA_1 A_2 \cdot e^{j\varphi_1}$ is located at the point $P(x_0, y_0)$, where $x_0 = E[I_{sum}]$ and $y_0 = E[Q_{sum}]$. The distance between P and the origin O is equal to $MA_1 A_2$. The angle between OP and the x axis is equal to the OPO (φ_1). While when noise is present, C_{sum} drifts to a random point $R(I_{sum}, Q_{sum})$. The angle between OP and OR represents the OPO estimation error $\Delta\varphi_1$. The distance between R and P (the line OP) is denoted by $\Delta l(\Delta s)$. Let's assume that $MA_1 A_2$ is sufficiently large that $MA_1 A_2 \gg \Delta l > \Delta s$. In this case $\Delta\varphi_1$ is very small and thus $\Delta\varphi_1$ can be estimated by

$$\Delta\varphi_1 \approx \tan\Delta\varphi_1 \approx \frac{\Delta s}{MA_1 A_2}. \tag{11}$$

The root mean square (RMS) of Δs and ΔI are related by the following equation

$$\Delta s^{rms} = \sqrt{\int_0^{\infty} \left(\int_0^{\Delta I} \Delta s^2 \frac{d\Delta s}{\Delta I} \right) P_{\Delta I} d\Delta I} = \sqrt{\frac{1}{3} \int_0^{\infty} \Delta I^2 P_{\Delta I} d\Delta I} = \frac{\Delta I^{rms}}{\sqrt{3}}. \tag{12}$$

The RMS of ΔI is equal to

$$\begin{aligned} \Delta I^{rms} &= \sqrt{\left\langle (I_{sum} - x_0)^2 + (Q_{sum} - y_0)^2 \right\rangle} = \sqrt{\left\langle (I_{sum} - E[I_{sum}])^2 \right\rangle + \left\langle (Q_{sum} - E[Q_{sum}])^2 \right\rangle} \\ &= \sqrt{D(I_{sum}) + D(Q_{sum})}. \end{aligned} \tag{13}$$

According to Eqs. (11–13), the RMS of $\Delta\varphi_1$, i.e., the root mean square error (RMSE), is approximately equal to

$$\Delta\varphi_1^{rms} \approx \mu \frac{\Delta s^{rms}}{MA_1A_2} = \mu \sqrt{\frac{2\left(\frac{\sigma_1^2}{A_1^2} + \frac{\sigma_2^2}{A_2^2} + 2\frac{\sigma_1^2}{A_1^2}\frac{\sigma_2^2}{A_2^2}\right)}{3M}}. \tag{14}$$

Here μ is a calibration factor related to the profile of the filters used in the receiver. When estimation error is present, the amplitude of the signal obtained after coherent combining (denoted by U_2) is given by

$$A_{U_2} = \left| A_1 + A_2 e^{j\Delta\varphi_1} \right| = A_1 \left| 1 + k_{2,1} e^{j\Delta\varphi_1} \right|. \tag{15}$$

Here $k_{2,1} = A_2/A_1$. The total noise power appearing in U_2 is equal to

$$\sigma_{U_2}^2 = 2\left(\sigma_1^2 + \sigma_2^2\right). \tag{16}$$

According to Eqs. (5, 15, 16), the actual SNR and equivalent input OSNR after DCC has the following form

$$SNR_{U_2} = \frac{A_{U_2}^2}{\sigma_{U2}^2} = \frac{A_1^2 \left| 1 + k_{2,1} e^{j\Delta\varphi_1} \right|^2}{2\left(\sigma_1^2 + \sigma_2^2\right)} = \gamma OSNR_{U_2}. \tag{17}$$

Thus the combining loss (CL) is given by

$$\begin{aligned} \Delta OSNR_{U_2} &= \left| \frac{1 + k_{2,1} e^{j\Delta\varphi_1}}{1 + k_{2,1}} \right|^2 \approx \left| \frac{1 + k_{2,1}(1 + j\Delta\varphi_1)}{1 + k_{2,1}} \right|^2 \\ &= \left(\frac{1}{1 + k_{2,1}} \right)^2 \left[(1 + k_{2,1})^2 + (k_{2,1}\Delta\varphi_1)^2 \right]. \end{aligned} \tag{18}$$

Eq. (18) shows that CL is a function of a random variable $\Delta\varphi_1$. Let's assume that $P_{\Delta\varphi_1}$ is the probability distribution function of $\Delta\varphi_1$. The averaged CL is given by

$$\begin{aligned} \left\langle \Delta OSNR_{U_2} \right\rangle &\approx \left(\frac{1}{1 + k_{2,1}} \right)^2 \int_{-\infty}^{+\infty} \left[(1 + k_{2,1})^2 + (k_{2,1}\Delta\varphi_1)^2 \right] P_{\Delta\varphi_1} d\Delta\varphi_1 \\ &= \left(\frac{1}{1 + k_{2,1}} \right)^2 \left[(1 + k_{2,1})^2 + {k_{2,1}}^2 \int_{-\infty}^{+\infty} {\Delta\varphi_1}^2 P_{\Delta\varphi_1} d\Delta\varphi_1 \right] \\ &= \left(\frac{1}{1 + k_{2,1}} \right)^2 \left[(1 + k_{2,1})^2 + \left(k_{2,1}{\Delta\varphi_1}^{rms}\right)^2 \right] \approx \left| \frac{1 + k_{2,1} e^{j{\Delta\varphi_1}^{rms}}}{1 + k_{2,1}} \right|. \end{aligned} \tag{19}$$

In summary, with Eqs. (14) and (19) we can predict the OPO estimation RMSE and the average CL according to the value of M.

For the $(n-1)$-th DCC, the analytical expression of the OPO estimation RMSE $\Delta\varphi_{n-1}^{rms}$ can be deduced by using the above method recursively. After some straight-forward but tedious algebra the expression of $\Delta\varphi_{n-1}^{rms}$ is found to be

$$\Delta\varphi_{n-1}^{rms} = \mu\sqrt{\frac{2}{3}\frac{\frac{\frac{\sigma_1^2}{A_1^2}+\sum_{i=1}^{n-1}k_{i,1}^2\frac{\sigma_i^2}{A_i^2}}{\left|1+\sum_{i=1}^{n-1}k_{i,1}e^{j\Delta\varphi_i^{rms'}}\right|^2}+\frac{\sigma_n^2}{A_n^2}+2\frac{\sigma_n^2}{A_n^2}\frac{\frac{\sigma_1^2}{A_1^2}+\sum_{i=1}^{n-1}k_{i,1}^2\frac{\sigma_i^2}{A_i^2}}{\left|1+\sum_{i=1}^{n-1}k_{i,1}e^{j\Delta\varphi_i^{rms'}}\right|^2}}{M}}.(2\le n\le N) \tag{20}$$

Here $k_{i,1}$ and $\Delta\varphi_i^{rms'}$ are defined as

$$k_{i,1} = \begin{cases} 0\ (i=1) \\ \frac{A_i}{A_1}\ (2\le i\le N-1) \end{cases}, \tag{21}$$

$$\Delta\varphi_i^{rms'} = \Delta\varphi_i^{rms} + \sum_{j=1}^{i}\alpha_j. \quad (1\le i\le N-1) \tag{22}$$

In Eq. (22) $\sum\alpha_j$ represents the angle between vector U_j and the x axis, α_j represents the angle between vector U_j and vector U_{j-1}. A_{Uj} represents the amplitude given by the following equations.

$$\alpha_j = \begin{cases} 0\ (j=1) \\ \arctan\left(\frac{A_j\sin\Delta\varphi_{j-1}^{rms}}{A_{U_{j-1}}+A_j\cos\Delta\varphi_{j-1}^{rms}}\right)\ (2\le j\le N-1) \end{cases}, \tag{23}$$

$$A_{U_j} = \begin{cases} A_1\ (j=1) \\ \left|A_1+\sum_{i=2}^{j}A_ie^{j\Delta\varphi_{i-1}^{rms'}}\right|\ (2\le j\le N) \end{cases}. \tag{24}$$

By using Eq. (18–19) recursively the averaged CL of the DCC of N branches of signals can be expressed by

$$\left\langle\Delta OSNR_{U_N}\right\rangle = \left|\frac{1+\sum_{i=2}^{N}k_{i,1}e^{j\Delta\varphi_{i-1}^{rms'}}}{1+\sum_{i=2}^{N}k_{i,1}}\right|^2.(N\ge 2) \tag{25}$$

3. Numerical Simulations

The setup of the numerical simulation system is shown in Fig. 1. The optical signal is 10 Gbps NRZ-BPSK signal. A random OPO between $-\pi$ and π is introduced in each version of optical signals to be combined by the optical delay lines. Due to atmospheric turbulence, the power received by different apertures spaced apart by a distance larger than the atmosphere phase correlation length can include more than 30 dB fades [9]. For this reason, the OSNR values of the input signals are varied by more than 33 dB via ASE noise loading before the receiver. The lower limit of the OSNR variation range is as low as -20 dB. This OSNR regime is often not interesting for normal DCRs used in optical fiber communication systems, but is of particular interest for the DCC based DCRs [9]. In each branch, a fourth order Gauss optical band-pass filter (OBPF) with 20 GHz 3-dB bandwidth is used before the DCR to mitigate the out-of-band ASE noise. In the DCR a fourth order Gauss low pass filter with 10 GHz 3-dB bandwidth is used extracted the electrical signal after the photodiode. In the simulation μ is set to be 1.2. The LO power is set to be equal to 10 dBm to overcome the receiver background noise. The laser frequency offset (LFO) and laser linewidth are equal to 500 MHz and 10 kHz, respectively.

To validate the analytical expressions presented, we first investigate the cases when $N=2$ and the prescribed CL is set to be equal to 0.1 and 0.5 dB, respectively. Fig. 4(a) shows the variations of the allowable OPO estimation RMSE ($\Delta\varphi_1^{rms}$) for CL = 0.1 dB obtained by Eq. (25) as a function of the OSNR values (in dB) of the two input signals to be combined. As we can see, the contour

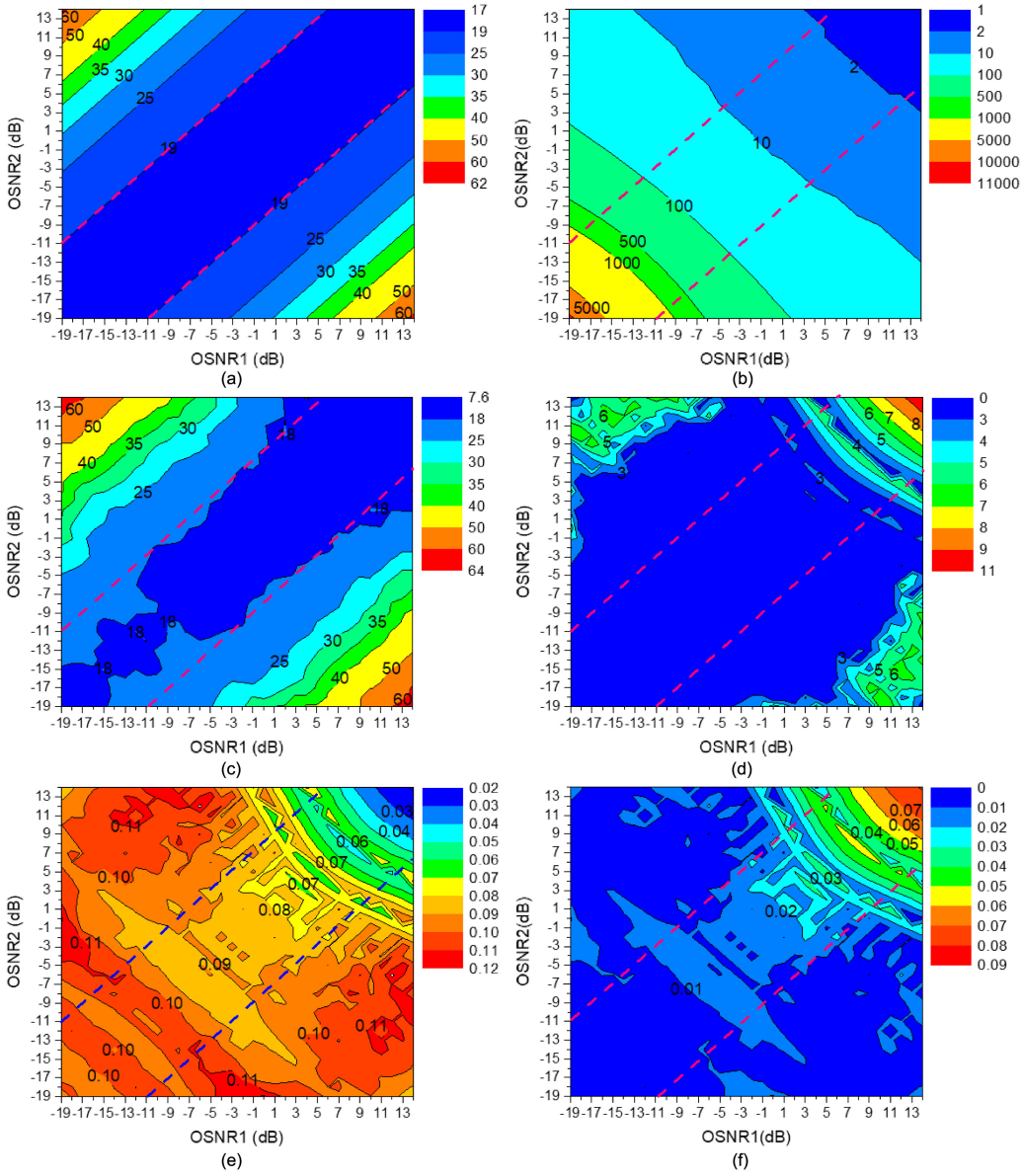

Fig. 4. The variations of the allowable $\Delta\varphi_1^{rms}$ (a) and corresponding M (b) for CL = 0.1 dB obtained by analytical expressions as a function of the OSNR values of the two input signals to be combined. (c) shows the real $\Delta\varphi_1^{rms}$ obtained by Monte Carlo simulations when M is set to be the corresponding values given in (b). (d) shows the difference between (a) and (c). (e) shows the real CL obtained by Monte Carlo simulations when M is set to be the corresponding values given in (b). (f) shows the difference between the real CL and the prescribed CL (0.1 dB).

lines are parallel to the line represented by $y = x + b$, where b stands for the difference between x and y. This is because, as can be seen from Eq. (25), for a given averaged CL ($\langle\Delta OSNR_{U_2}\rangle$), $\Delta\varphi_1^{rms}$ is only determined by $k_{2,1} = A_2/A_1$ which actually stands for the OSNR difference (in dB) between the two signals. Fig. 4(b) shows the variations of M obtained by Eq. (20) for CL = 0.1 dB as a function of the OSNR values. As we can see, the contour lines are approximately parallel to the line represented by $y = -x + c$, where c stands for the sum of x and y. It proves that M is determined by the overall quality of the two input signals to be phase aligned. In the upper right corner both OSNR values are very high, and thus M is as low as 1, while in the lower left

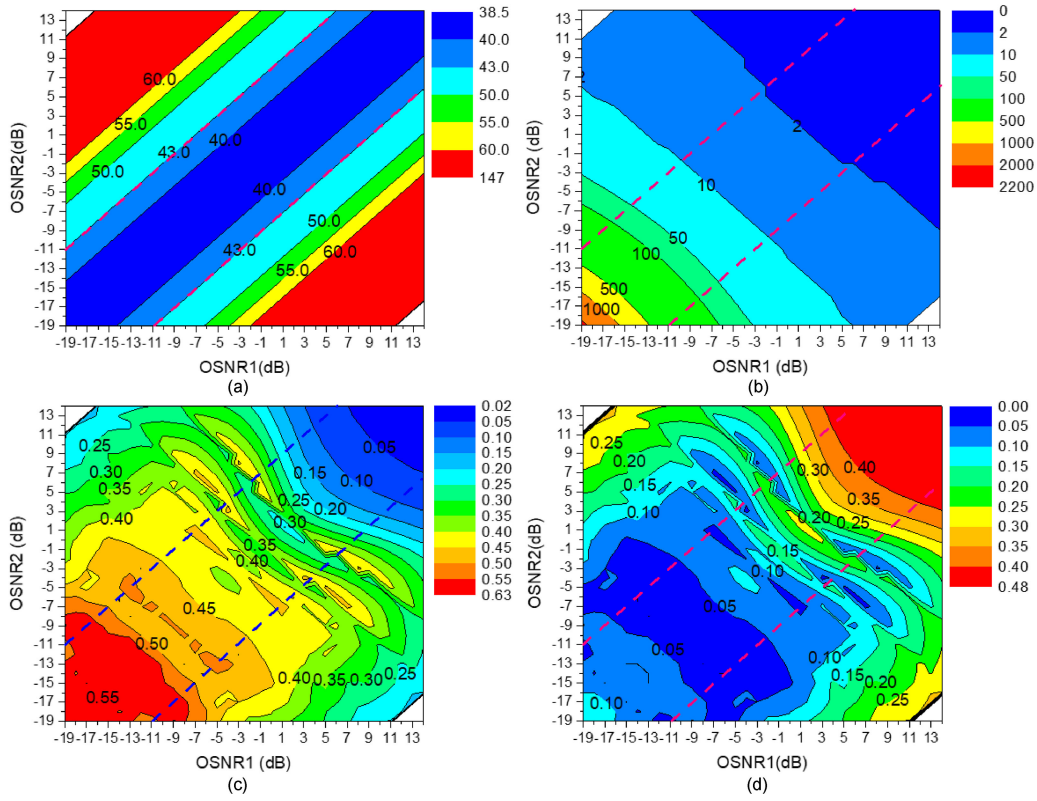

Fig. 5. The variations of the allowable $\Delta\varphi_1^{rms}$ (a) and corresponding M (b) for CL = 0.5 dB obtained by analytical expressions as a function of the OSNR values of the two input signals to be combined. (c) shows the real CL obtained by Monte Carlo simulations when M is set to be the corresponding values given in (b). (d) shows the difference between the real CL and the prescribed CL(0.5 dB).

corner both OSNR values are very low, and thus M is as high as 5000. It is noteworthy that the maximum number of symbols that can be used for the estimation must have a total duration less than the atmospheric coherence time and laser coherence time [21]. The former is a function of the particular atmospherics and is on the order of ∼1 to 10 ms. The latter is ∼100 μs for a 10 kHz linewidth. In the simulations M is not larger than 11000 and the duration of 11000 symbols for the 10 Gbps NRZ-BPSK signal is 1.1 μs. It is much smaller than the coherence times, and thus the simulation results are valid considering these practical limitations.

Fig. 4(c) shows the real $\Delta\varphi_1^{rms}$ obtained by Monte Carlo simulations when M is set to be the corresponding values given in Fig. 4(b). To obtain the real $\Delta\varphi_1^{rms}$, 500 times of Monte Carlo simulations are carried out for each data point under random ASE noise pattern. As we can see, the contour lines are also approximately parallel to the line $y = x + b$ as in Fig. 4(a). Fig. 4(d) shows the difference between Fig. 4(a) and 4(c). As we can see, the deviation is lower than 5 degree in most areas except the upper left and lower right corners where $\Delta\varphi_1^{rms}$ is larger than 40 degrees. This is because the assumption that $MA_1A_2 \gg \Delta I > \Delta s$ is not valid when $\Delta\varphi_1^{rms}$ is too large. However, in these two corners, the OSNR difference between the two signals to be combined is very large (about 20 dB). In this case, EGC will result in a negative net OSNR gain (introducing more noise) and should not be conducted [20], and thus the two corners are not of interest for the EGC based DCC. As regard to the upper right corner, the relatively large deviation is due to the rounding up error which is not neglectable when M obtained by Eq. (20) is not a integer and as small as 1 (see Fig. 4(b)). However, because of the rounding up operation, M is always larger than the value required, thus still guaranteeing that the real CL is lower than the prescribe CL.

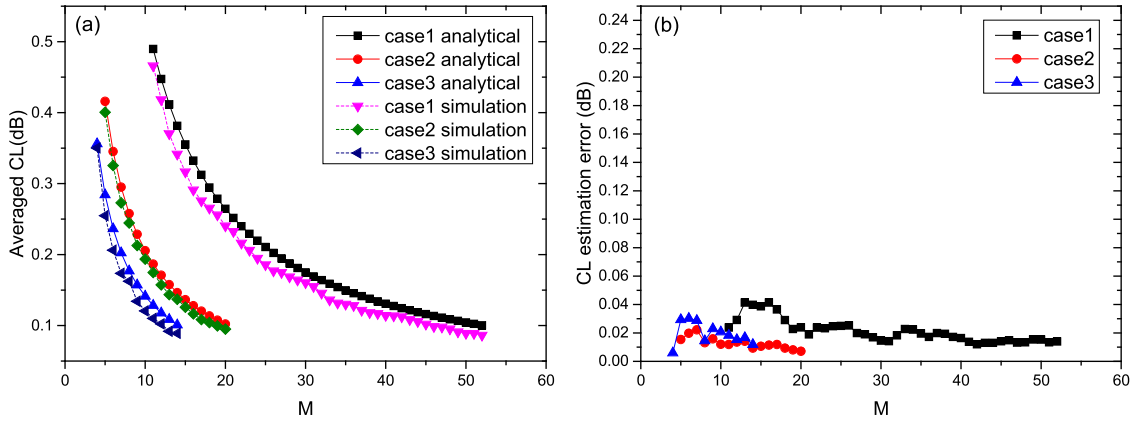

Fig. 6. (a) The variations of the CL as a function of M when N = 4. For case 1, 2 and 3 the OSNRs of the four signals to be combined are [−4 −5 −6 −7] dB, [1 −4 −5 −9] dB and [0 −4 −9 −10] dB, respectively. (b) The difference between the analytical and numerical results.

Fig. 4(e) shows the real CL obtained by Monte Carlo simulations when M is set to be the corresponding values given in Fig. 4(b). As we can see, the real CL is close to 0.1 dB in most areas. The deviation of the real CL from the prescribe CL of 0.1 dB is shown in Fig. 4(f). In most areas the deviation is smaller than 0.03 dB except the upper right corner due to the rounding up error. However, as we can see from Fig. 4(e), in this corner the real CL is actually smaller than the prescribed value (0.1 dB), thus can still satisfy the requirement.

Fig. 5(a) and (b) show the variations of the allowable $\Delta\varphi_1^{rms}$ and corresponding M for CL = 0.5 dB obtained by Eq. (20) and (25) as a function of the OSNR values of the two input signals to be combined. The contour lines in the two figures have similar characteristics as those in Fig. 4(a) and (b). But as the prescribed CL is larger, the allowable $\Delta\varphi_1^{rms}$ is also larger. For example, for the given OSNR difference of 8 dB (represented by the red dashed lines), the allowable $\Delta\varphi_1^{rms}$ is 19 and 43 degrees in Fig. 4(a) and Fig. 5(a), respectively. As the required $\Delta\varphi_1^{rms}$ is larger, M required for CL = 0.5 dB is greatly reduced compared with the case when CL = 0.1 dB. For example, the upper limit appearing in the lower left corner of Fig. 4(b) is as large as 5000, while it is only 1000 in Fig. 5(b). Fig. 5(c) shows the real CL obtained by Monte Carlo simulations when M is set to be the corresponding values given in Fig. 5(b). As can be seen, the real CL is close to 0.5 dB in most areas. The deviation of the real CL from the prescribe value is shown in Fig. 5(d). In most areas the deviation is smaller than 0.1 dB except the upper left, lower right and upper right corners. The overall deviation is larger than those shown in Fig. 4(f) because $\Delta\varphi_1^{rms}$ required for CL = 0.5 dB is larger than that required for CL = 0.1 dB. We note that, as explained above, the upper left and lower right corners are not of interest for the EGC based DCC because EGC will introduce more noise when the OSNR difference between the two signals is about 20 dB. In the upper right corner, the rounding up operation leads to the relatively large deviation as M is very small in the area, but it can still guarantee CL below the prescribed CL as shown in Fig. 5(a).

Fig. 6(a) shows the variations of the CL as a function of M when $N = 4$. The OSNR values of the four signals to be combined are randomly selected from a large range. The investigated cases include [−4 −5 −6 −7] dB, [1 −4 −5 −9] dB and [0 −4 −9 −10] dB (hereafter referred to as case 1, 2 and 3, respectively). Both analytical and numerical results are presented in Fig. 6(a) for comparison. Noting that EGC is performed from signals with higher OSNRs to signals with lower OSNRs provided that the net gain after EGC is positive. Here the variation range of M is chosen to guarantee CL adjustment from 0.1 to 0.5 dB. In the numerical simulation the averaged CL is obtained from 300 times of Monte Carlo simulations with different ASE noise patterns. As we can see, the averaged CL decreases with increasing M. Thus, selecting a proper M value can satisfy different prescribed CL and computation complexity requirements. For example, for case 1, the

computation complexity can be reduced by about 80% when the allowable CL is relaxed from 0.1 to 0.5 dB. As we can see, the analytical and numerical results agree very well for all of the cases. The difference between the real CL and prescribe CL is shown in Fig. 6(b). The maximal error is lower than 0.05 dB. Furthermore, as we can see, the error is even lower (lower than 0.02 dB) at the tails of the curves where the prescribed CL is reduced to 0.1 dB (see Fig. 6(a)). This is because when CL is smaller, the allowable OPO estimation error is smaller, and thus the analytical expressions are more accurate.

4. Conclusion

In this paper we investigate the relationship between the computation complexity of the PAA, the OPO estimation error and the combining loss for the EGC based DCC technique. Analytical expressions are deduced to provide a simple procedure that gives the optimum value for M depending on the input OSNR and prescribed combining loss. The analytical results are validated by extensive numerical simulations. This work can provide useful guidelines for low computation complexity phase alignment in the EGC based FSOC system providing exceptionally high sensitivity.

References

[1] D. M. Boroson *et al.*, "Overview and results of the lunar laser communication demonstration," *Proc. SPIE*, vol. 8971, 2014, Art. no. 89710S.
[2] D. M. Cornwell, "NASA's optical communications program for 2015 and beyond," in *Proc. IEEE Int. Conf. Space Opt. Syst. Appl.*, 2015, pp. 10–14.
[3] R. W. Kingsbury, D. O. Caplan, and K. L. Cahoy, "Compact optical transmitters for CubeSat free-space optical communications," *Proc. SPIE*, vol. 9354, 2015, Art. no. 93540S.
[4] H. Hemmati, *Deep Space Optical Communications*. Hoboken, NJ, USA: Wiley, 2006.
[5] D. O. Caplan, "Laser communication transmitter and receiver design," *J. Opt. Fiber Commun.* vol. 4, no. 4-5, pp. 225–362, 2007.
[6] H. Hemmati and D. O. Caplan, "Optical satellite communications," in *Optical Fiber Telecommunications.* 6th ed., I. P. Kaminow, T. Li, and A. E. Willner, Eds., Amsterdam, The Netherlands: Elsevier, 2013.
[7] D. J. Geisler *et al.*, "Multi-aperture digital coherent combining for free-space optical communication receivers," *Opt. Exp.*, vol. 24, no. 12, pp. 12661–12671, 2016.
[8] T. M. Yarnall, D. J. Geisler, M. L. Stevens, C. M. Schieler, B. S. Robinson, and S. A. Hamilton, "Multi-aperture digital coherent combining for next-generation optical communication receivers," in *Proc. IEEE Int. Conf. Space Opt. Syst. Appl.*, 2015, pp. 1–6.
[9] D. J. Geisler *et al.*, "Experimental demonstration of multi-aperture digital coherent combining over a 3.2-km free-space link," *Proc. SPIE*, vol. 10096, 2017, Art. no. 100960C.
[10] H. P. Stahl, "Survey of cost models for space telescopes," *Opt. Eng.*, vol. 49, no. 5, pp. 053005.1–053005.8, 2010.
[11] S. Shaklan and F. Roddier, "Coupling starlight into single-mode fiber optics," *Appl. Opt.*, vol. 27, no. 11, pp. 2334–2338, 1988.
[12] R. Tyson, *Principles of Adaptive Optics*. 3rd ed., Boca Raton, FL, USA: CRC Press, 2011.
[13] J. Xu *et al.*, "Experimental comparison of coherent array detection and conventional coherent detection for laser radar and communications," *Proc. SPIE*, vol. 3615, pp. 300–309, 1999.
[14] A. R. Weeks *et al.*, "Experimental verification and theory for an eight-element multiple-aperture equal-gain coherent laser receiver for laser communications," *Appl. Opt.*, vol. 37, no. 21, pp. 4782–4788, 1998.
[15] C. M. Stickley *et al.*, "Demonstration of an adaptive, coherent-combining laser radar receiver," in *Advances in Atmospheric Remote Sensing with Lidar*. Berlin, Germany: Springer, 1997, pp. 247–250.
[16] P. Gatt *et al.*, "Coherent optical array receivers for the mitigation of atmospheric turbulence and speckle effects," *Appl. Opt.*, vol. 35, no. 30, pp. 5999–6009, 1996.
[17] Y. Yang *et al.*, "Multi-aperture all-fiber active coherent beam combining for free-space optical communication receivers," *Opt. Exp.*, vol. 25, no. 22, pp. 27519–27532, 2017.
[18] M. S. Faruk, Y Mori, and K. Kikuchi, "Estimation of OSNR for Nyquist-WDM transmission systems using statistical moments of equalized signals in digital coherent receivers," in *Proc. IEEE OFC*, 2014, pp. 1–3.
[19] I. P. Kaminow, T. Li, and A. E. Willner, *Optical Fiber Telecommunications VB: Systems and Networks*. Amsterdam, The Netherlands: Elsevier, 2010.
[20] M. Niu, J. Cheng, and J. F. Holzman, "Exact error rate analysis of equal gain and selection diversity for coherent free-space optical systems on strong turbulence channels," *Opt. Exp.*, vol. 18, no. 13, pp. 13915–13926, 2010.
[21] D. J. Geisler *et al.*, "Demonstration of a variable data-rate free-space optical communication architecture using efficient coherent techniques," *Opt. Eng.*, vol. 55, no. 11, 2016, Art. no. 111605.